Chemical Engineering Journal 154 (2009) 281–286

Contents lists available at ScienceDirect

Chemical Engineering Journal

journal homepage: www.elsevier.com/locate/cej

Hydrogen production by steam reforming of dimethyl ether over Cu–Zn/CeO_2–ZrO_2 catalytic monoliths

Cristian Ledesma, Jordi Llorca*

Institut de Tècniques Energètiques, Universitat Politècnica de Catalunya, Av. Diagonal 647, Ed. ETSEIB, 08028 Barcelona, Spain

ARTICLE INFO

Article history:
Received 3 December 2008
Received in revised form 19 February 2009
Accepted 29 March 2009

Keywords:
Hydrogen
Dimethyl ether
Steam reforming
Catalytic monolith
Copper–zinc catalyst

ABSTRACT

Several catalytic monoliths containing Cu, Zn, or Cu–Zn supported on CeO_2, ZrO_2, or CeO_2–ZrO_2 were prepared and tested for the dimethyl ether steam reforming reaction under a steam to carbon ratio of S/C = 1.5 at 473–823 K. The best catalytic performance in terms of stability, hydrogen yield, and low CO production was obtained over Cu–Zn/ZrO_2 catalytic monoliths (2.1×10^{-3} mol_{DME} h^{-1} g_{cat}^{-1} converted with $S_{H_2} = 96\%$ and $S_{CO_2} = 90\%$ at 753 K). Catalytic monoliths were characterized by XRD, SEM, EDX, NH_3-TPD as well as by long-term catalytic and mechanical stability tests.

1. Introduction

In recent years, the use of hydrogen for fuel cell applications has been regarded as one of the most efficient technologies for electricity generation or vehicle applications [1–5]. Steam reforming of fuels has attracted much attention as an efficient technology for hydrogen production because it provides a higher reformate quality (e.g. higher hydrogen production yield, lower rate of side reactions and by-products) when compared with partial oxidation or autothermal reforming [2,6–8]. Among several substrates, dimethyl ether (DME) can be stored and handled easily (it liquefies at about 6 bar) and is considered a promising candidate for reforming technologies since it may be easily derived from renewable biomass [4,5,9]. DME is thought to be an alternative to liquefied petroleum gas (LPG) due to their similar physical properties [3,10–13]. The relatively inert, non-corrosive and non-carcinogenic character of DME may help to promote its practical usage with respect to harmful methanol [12–16]. The steam reforming of DME is comprised by two consecutive reactions [2–5]. The first step is the hydrolysis of DME to form methanol over a solid acid catalyst (Eq. (1)). However, the use of too strong acidic materials should be avoided since they strongly promote the formation of carbonaceous residues, which results in rapid catalyst deactivation. The second step is the steam reforming of methanol (Eq. (2)), which is usually carried out over Cu-based catalysts. The overall reaction yields 6 mol H_2 per mol DME, and half of H_2 comes from water (Eq. (3)).

$$(CH_3)_2O + H_2O \rightarrow 2CH_3OH \quad \Delta H^\circ = +37\,kJ\,mol^{-1} \tag{1}$$

$$CH_3OH + H_2O \rightarrow CO_2 + 3H_2 \quad \Delta H^\circ = +49\,kJ\,mol^{-1} \tag{2}$$

$$(CH_3)_2O + 3H_2O \rightarrow 2CO_2 + 6H_2 \quad \Delta H^\circ = +135\,kJ\,mol^{-1} \tag{3}$$

Therefore, either a two-bed catalytic device or a bifunctional catalyst is required to carry out the steam reforming of DME. Mixtures of acidic oxides or zeolites and Pd, Pt or Cu–Zn-based systems have been reported in the literature as suited catalysts for DME steam reforming [1–3,16–20] and, as far as we know, there is only one work with catalytic monoliths using Pd–Pt–Zn-based systems supported on Al_2O_3 or zeolites for autothermal reforming of DME [17]. Monolithic supports can be an attractive replacement for conventional catalysts because they offer many advantages in terms of efficiency, cost and operation conditions [21]. In this work, we have tested the DME steam reforming reaction over honeycomb catalysts loaded with CeO_2-, ZrO_2- or $Ce_{0.5}Zr_{0.5}O_2$-supported Cu, Zn, or Cu–Zn. In addition to their mild acidic character, we have chosen these supports due to their redox properties. The present contribution provides the first example of DME steam reforming over honeycomb samples.

2. Experimental methods

2.1. Preparation of catalytic monoliths

400 cpsi (cells per square inch) cordierite monolith cylinders with a diameter of 2 cm and a length of 2 cm were used. They were

* Corresponding author. Tel.: +34 93 401 17 08; fax.: +34 93 401 71 49.
E-mail address: jordi.llorca@upc.edu (J. Llorca).

1385-8947/$ – see front matter © 2009 Elsevier B.V. All rights reserved.
doi:10.1016/j.cej.2009.03.055

obtained by cutting larger monolith pieces with a diamond saw. Monoliths were coated with Cu, Zn, or Cu–Zn particles supported on CeO_2, ZrO_2, or CeO_2–ZrO_2 (CeO_2:ZrO_2 = 1:1) by the washcoating method in two steps. First, CeO_2 and/or ZrO_2 were bound to the monoliths walls from aqueous solutions of $CeCl_3{\cdot}7H_2O$ and/or $ZrOCl_2{\cdot}8H_2O$ as precursors. Monoliths were dried at 373 K under continuous rotation and then calcined in air at 773 K for 2 h. This procedure was repeated several times in order to obtain the desired weight gain (10–12% w/w) of each support. Then, the active metals were loaded over the monoliths washcoated with the supports by incipient wetness impregnation from $Cu(NO_3)_2{\cdot}3H_2O$ and/or $Zn(NO_3)_2{\cdot}6H_2O$ ethanolic solutions. The resulting monoliths were finally dried at 373 K under continuous rotation and then calcined in air at 773 K for 2 h.

2.2. Characterization techniques

Mechanical stability of the honeycomb samples was evaluated by immersion in water and exposition to high frequency ultrasounds (40 kHz). Weight loss was monitored for 30 min. The microstructure, morphology and composition of monolith channels were studied by scanning electron microscopy (SEM) and energy dispersive X-ray analysis (EDX). Secondary electron images were recorded at 20 kV using a JEOL JSM 6400 instrument. Powder X-ray diffraction (XRD) was collected at a step width of 0.02° and by counting 10 s at each step with a Siemens D-500 instrument equipped with a Cu target and a graphite monochromator. Ammonia-temperature programmed desorption (NH_3-TPD) analysis were performed to measure catalysts acidity. Samples were first heated at 773 K under He during 10 min and then 9 mL min^{-1} NH_3 were passed over the samples at 323 K for 5 min. After that, He was flowed until no NH_3 signal was detected by mass spectrometry (MKS Cirrus) and, finally, NH_3-TPD was conducted up to 873 K at 10 K min^{-1}.

2.3. Catalytic tests

Dimethyl ether steam reforming was carried out at atmospheric pressure in a stainless steel tubular reactor under a weight hourly space velocity (WHSV) of 2–17 L h^{-1} $g_{cat}{}^{-1}$. DME (between 2.7×10^{-3} and 1.1×10^{-2} mol h^{-1}) and H_2O were fed separately at a steam to carbon ratio of S/C = 1.5 and the mixture was balanced with N_2. The effluent of the reactor was monitored on line with an Agilent 3000A micro-GC, which allowed a careful quantification of H_2, N_2, CO, CO_2, CH_4, CH_3OH, H_2O and CH_3OCH_3 concentrations. In a typical experiment, the catalytic monolith was first pretreated inside the reactor with a H_2:He mixture (50 mL min^{-1}, 10% H_2) at 573 K for 2 h. Then the temperature was lowered to 473 K under He flow and the reaction mixture was introduced at this temperature. The reaction was followed from 473 to 823 K (2 K min^{-1}). Monoliths operated under isothermal conditions as deduced from temperature monitoring inside the channels, located either in contact with the stainless steel housing wall or at the center of the reactor. Stability tests were conducted over 96 h.

Table 1
Catalytic monoliths prepared in this work. Chemical composition reported as weight percent with respect to monolith weight. Acidity values calculated from NH_3-TPD.

Catalyst	% Ce	% Zr	% Cu	% Zn	% w/w	mmol NH_3 $g_{cat}{}^{-1}$
Cu/CeO_2	13.2		4.5		17.8	
Zn/CeO_2	11.3			4.6	15.9	
$Cu–Zn/CeO_2$	13.6		5.4	6.5	25.4	
CeO_2	11.3				11.3	9.9
Cu/ZrO_2		12.0	4.7		16.7	0.9
Zn/ZrO_2		10.3		5.4	15.7	0.9
$Cu–Zn/ZrO_2$		10.6	4.0	5.2	19.8	1.2
$Cu–Zn(A)/ZrO_2$		10.4	2.1	2.5	15.0	0.9
$Cu–Zn(B)/ZrO_2$		9.6	6.2	7.3	23.1	0.8
$Cu–Zn(C)/ZrO_2$		11.9	7.8	9.7	29.4	0.8
ZrO_2		10.2			10.2	6.8
$Cu/CeO_2–ZrO_2$	6.4	6.4	5.3		18.1	
$Zn/CeO_2–ZrO_2$	6.3	6.2		4.8	17.3	
$Cu–Zn/CeO_2–ZrO_2$	5.9	5.9	4.0	4.9	20.7	
$CeO_2–ZrO_2$	5.3	5.2			10.5	3.1

3. Results and discussion

3.1. Structural characterization

Table 1 compiles all the catalytic monoliths prepared in this work, including chemical composition and acidity values. Mechanical stability of the catalytically active phase in monoliths is a critical issue for industrial application because coating loss and banking up should be completely avoided. In this regard, the weight loss of all the catalytic monoliths prepared in this work was about 1% after 30 min of ultrasound exposure, so the adherence of catalyst coatings was very high in all cases. The dispersion and homogeneity of the catalytic coatings were also monitored by scanning electron microscopy (SEM) and energy dispersive X-ray analysis (EDX). A representative SEM image corresponding to a single channel of a monolith coated with ZrO_2 is shown in Fig. 1a. The picture shows a very good dispersion and homogeneity of the zirconia coating. A similar good dispersion and homogeneity was observed for the monolith coated with Cu/ZrO_2 catalyst. Bright areas in Fig. 1b correspond to Cu-rich domains. In contrast, the dispersion of Zn in $Cu–Zn/ZrO_2$ was poorer as a result of the existence of Zn-rich aggregates (Fig. 1c). However, a careful EDX analysis indicated that the occurrence of Cu is always associated with the presence of Zn, meaning that an intimate contact exists between the two metals.

3.2. Acidity measurements

Since the first step of the dimethyl ether steam reforming is the hydration into methanol and this step is strongly influenced by the acidity of the catalyst, we have determined the acidity directly over our monoliths using the NH_3-TPD technique, as explained in Sec-

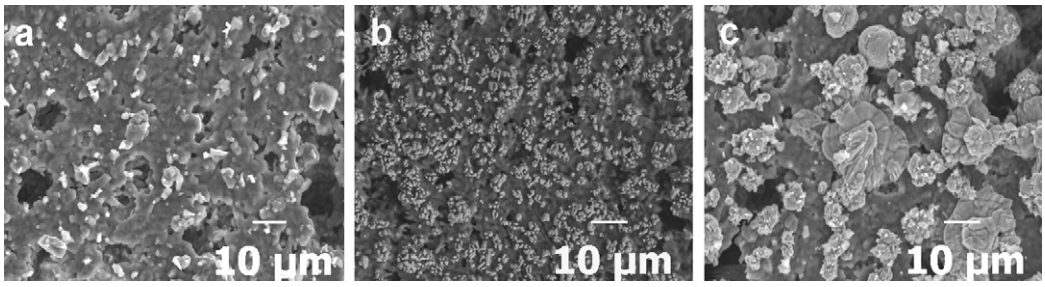

Fig. 1. Scanning electron microscopy images corresponding to a single channel of a monolith coated with ZrO_2 (a), Cu/ZrO_2 (b) and $Cu–Zn/ZrO_2$ (c).

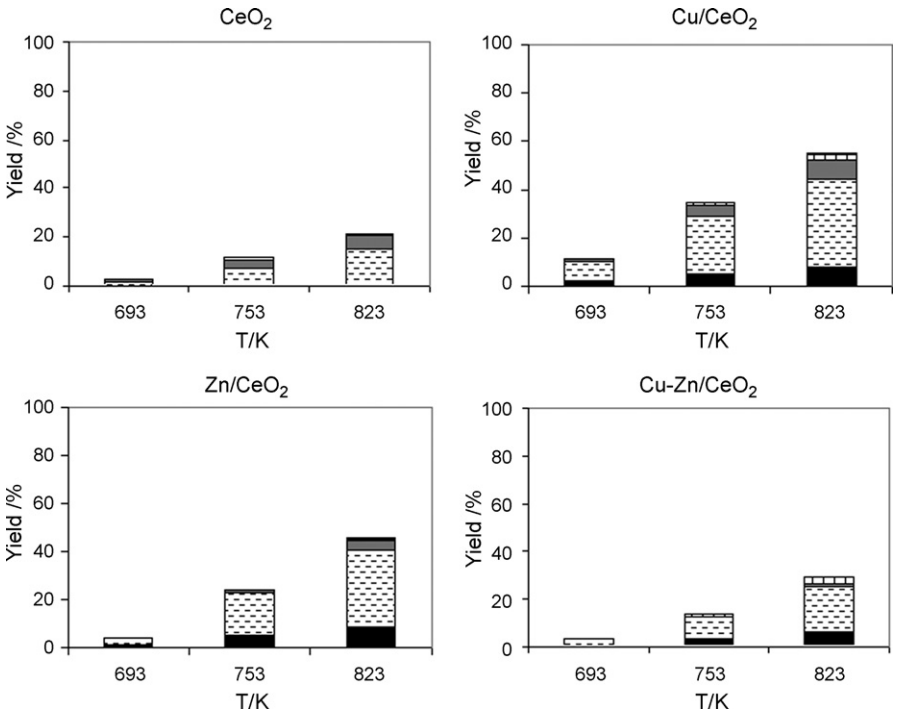

Fig. 2. Catalytic performance of CeO_2-based monoliths under DME steam reforming conditions (■ = CO_2, ▨ = H_2, ▩ = CO, ▥ = CH_4 and □ = CH_3OH). Experimental conditions: 2.7×10^{-3} mol_{DME} h^{-1}, S/C = 1.5 and WHSV ~16.6 L h^{-1} $g_{cat}{}^{-1}$.

tion 2.2. Table 1 lists the acidity values in terms of mmol adsorbed NH_3 $g_{cat}{}^{-1}$. Among the supports, CeO_2 had the highest acidity value, followed by ZrO_2 and CeO_2–ZrO_2. In order to understand the unexpected low acidity value recorded over CeO_2–ZrO_2 (an intermediate acidity between that of CeO_2 and ZrO_2 was expected) we carried out an X-ray study directly over the catalytic monoliths. It is well known that ZrO_2 can exhibit different crystal structures (monoclinic and tetragonal) and that ZrO_2–CeO_2 mixtures can also result in a cubic crystal structure [22–24]. In the X-ray diffraction profile of the ZrO_2 catalytic monolith there was a peak at 31°, which is ascribed to the (1 0 1) crystallographic plane of tetragonal ZrO_2, whereas no peak characteristic of monoclinic ZrO_2 was detected around 24°. In contrast, the X-ray diffraction profile of the CeO_2–ZrO_2 catalytic monolith showed peaks likely due to the cubic structure. The mean

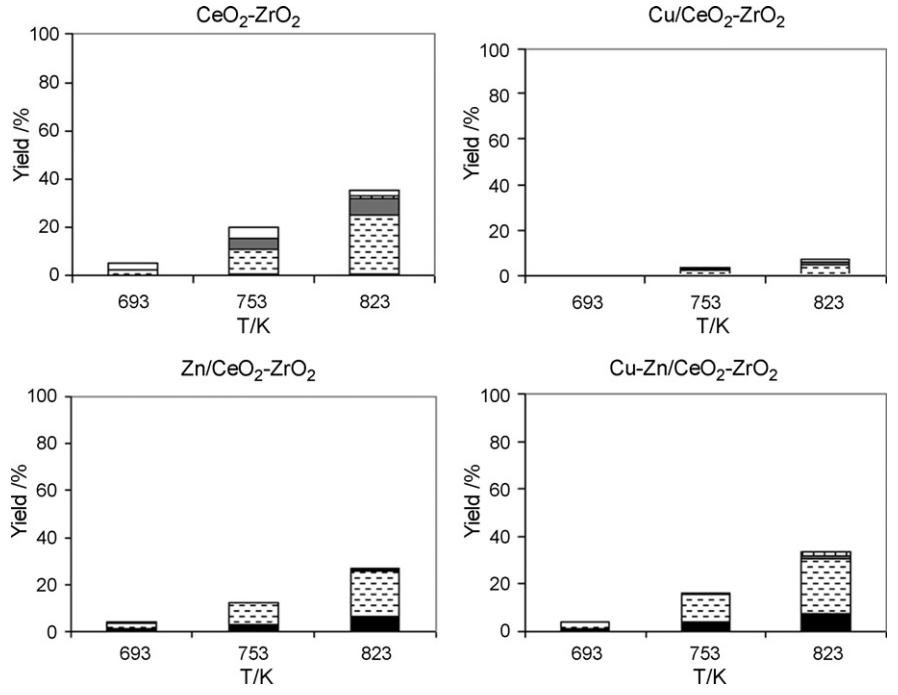

Fig. 3. Catalytic performance of CeO_2–ZrO_2-based monoliths under DME steam reforming conditions (■ = CO_2, ▨ = H_2, ▩ = CO, ▥ = CH_4 and □ = CH_3OH). Experimental conditions: 2.7×10^{-3} mol_{DME} h^{-1}, S/C = 1.5 and WHSV ~16.6 L h^{-1} $g_{cat}{}^{-1}$.

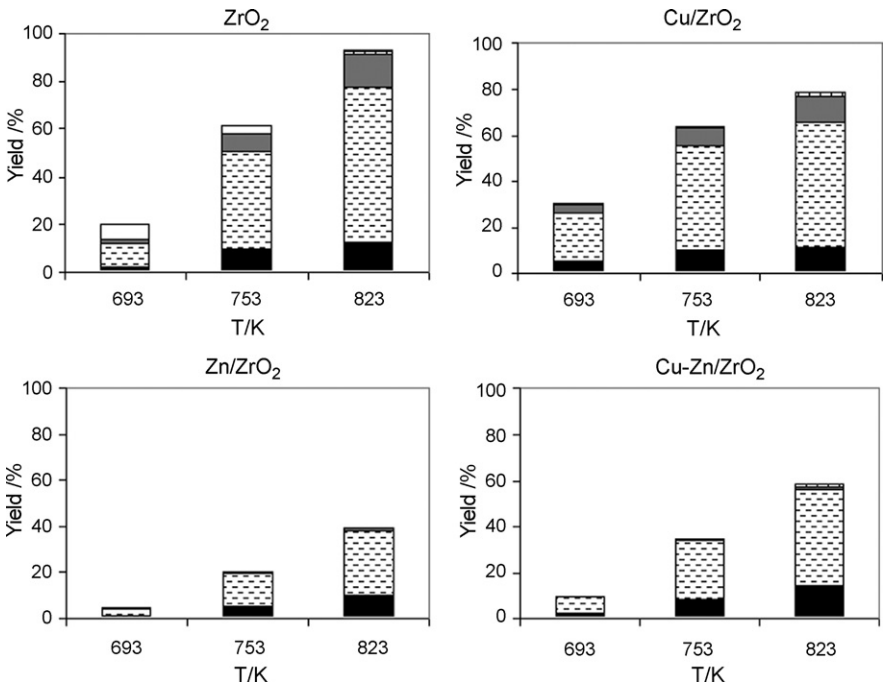

Fig. 4. Catalytic performance of ZrO_2-based monoliths under DME steam reforming conditions (■ = CO_2, ▨ = H_2, ▩ = CO, ▥ = CH_4 and □ = CH_3OH). Experimental conditions: 2.7×10^{-3} mol_{DME} h^{-1}, S/C = 1.5 and WHSV ~16.6 L h^{-1} $g_{cat}{}^{-1}$.

crystallite size calculated from line broadening in ZrO_2 was about 18 nm, whereas that of ZrO_2–CeO_2 was below 4 nm. Therefore, the different acidity of these catalytic monoliths is not related to differences in surface area and may be due to the different crystal structure of CeO_2–ZrO_2 and ZrO_2. The addition of Cu, Zn or Cu–Zn to the monoliths coated with the supports decreased the acidity values in all cases, as expected. The acidity values of catalytic monoliths with Cu, Zn or Cu–Zn for a given support were similar.

3.3. Dimethyl ether steam reforming

All the monoliths prepared in this work were tested in the DME steam reforming reaction at 473–823 K under diluted conditions in order to establish accurate comparisons in their catalytic performance without diffusional or mass-transfer limitations. These conditions were set as 2.7×10^{-3} mol_{DME} h^{-1}, S/C = 1.5 and WHSV ~16.6 L h^{-1} $g_{cat}{}^{-1}$. Figs. 2–5 show the yields attained for all prod-

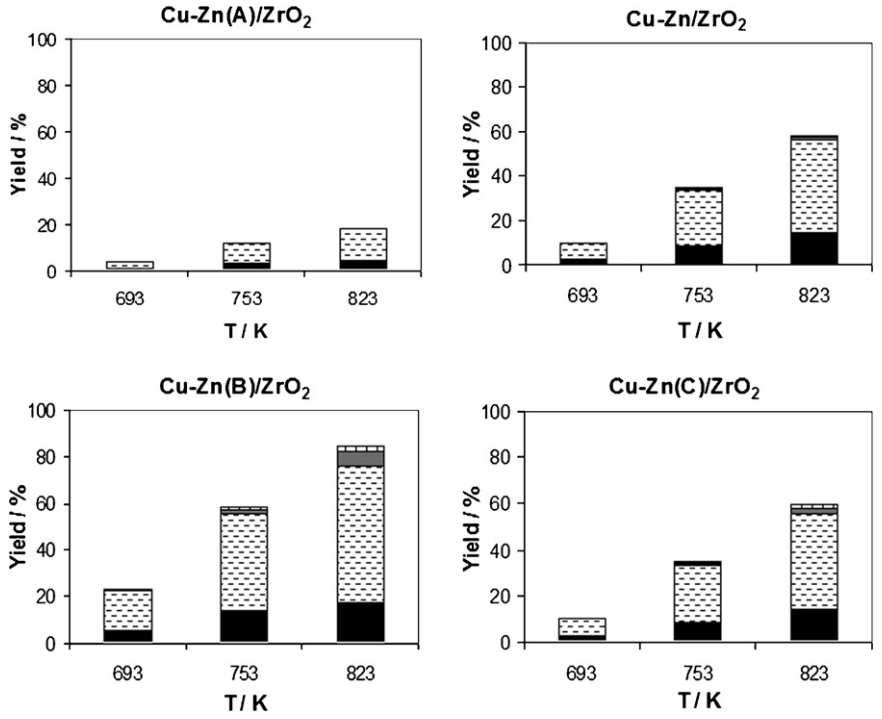

Fig. 5. Catalytic performance of Cu–Zn/ZrO_2 monoliths with different metal loadings under DME steam reforming conditions (■ = CO_2, ▨ = H_2, ▩ = CO, ▥ = CH_4 and □ = CH_3OH). Experimental conditions: 2.7×10^{-3} mol_{DME} h^{-1}, S/C = 1.5 and WHSV ~16.6 L h^{-1} $g_{cat}{}^{-1}$.

ucts on a dry basis at three selected temperatures (693, 753, and 823 K) for each family of catalytic monoliths with the same support. Catalytic monoliths based on CeO_2 (Fig. 2) clearly showed the effect of Cu and Zn addition. The monolith containing only CeO_2 was active for DME transformation mainly into a mixture of H_2 and CO, with $[H_2]\sim 2[CO]$, meaning that the CeO_2 sample was active for both the hydration of DME into methanol due to the presence of acidic centers and methanol decomposition (Eq. (4)). However, the minute amount of CO_2 at the outlet stream indicated that the water gas shift reaction (WGS) between CO and steam (Eq. (5)) was largely hindered.

$$CH_3OH \rightarrow CO + 2H_2 \quad (4)$$

$$CO + H_2O \rightarrow CO_2 + H_2 \quad (5)$$

In contrast, the addition of Cu and/or Zn promoted the WGS and the selectivity towards H_2 and CO_2 increased notably, although CO still remained among the products of the reaction. The addition of Cu or Zn also resulted in a marked increase of DME transformation with respect to the monolith coated with CeO_2 alone, but in the case of the monolith with Cu–Zn/CeO_2, the increase of activity was negligible probably because the DME hydration into methanol was affected by the decrease of acidity upon metal loading. Catalytic monoliths based on CeO_2–ZrO_2 showed a similar selectivity trend (Fig. 3), although the appearance of methanol among the reaction products in the monolith coated with CeO_2–ZrO_2 alone indicates that the sample was less active for the second step of the DME reforming, that is, the methanol transformation. In this case, the addition of Zn strongly promoted the WGS reaction, but due to the low intrinsic acidity of the CeO_2–ZrO_2 support (Table 1), samples loaded with metal exhibited lower activity, particularly the Cu/CeO_2–ZrO_2 sample.

Catalytic monoliths based on ZrO_2 were much more active than those based on CeO_2 or CeO_2–ZrO_2 (Fig. 4). Over ZrO_2, the transformation of DME into a mixture containing CH_3OH, H_2, CO and CO_2 occurred to a large extent, and DME conversion values greater than 90% were attained at high temperature. The ratio between H_2, CO, and CO_2 follows the trend: $[H_2]\sim 2.2[CO] + 2.4[CO_2]$ and $[CO]/[CO_2]\sim 1.1$, which corresponds to a scheme where methanol decomposition (Eq. (4)) occurs at a extent of ~75% followed by WGS reaction (Eq. (5)) at a extent of ~25%. The addition of Cu to ZrO_2 resulted in the disappearance of methanol among the reaction products due to the promotion of methanol transformation in the presence of Cu, but the selectivity towards H_2, CO and CO_2 remained approximately unchanged, with an increasing amount of CO at increasing temperature due to the reverse-WGS reaction. In contrast, the addition of Zn to ZrO_2 resulted in a strong change in selectivity and almost exclusively H_2 and CO_2 with $[H_2]\sim 3[CO_2]$ were encountered at the reactor outlet at all temperature tested. The promotional effect of Zn for the WGS reaction is in accordance to other results in methanol steam reforming [25–29]. However, the activity of the Zn/ZrO_2 sample was low with respect to monoliths ZrO_2 and Cu/ZrO_2. A compromise situation between activity and selectivity is encountered with the catalytic monolith Cu–Zn/ZrO_2, where a good selectivity was maintained at intermediate conversion levels. Therefore, the catalytic performance in the DME steam reforming reaction was further studied over several Cu–Zn/ZrO_2 catalytic monoliths with different metal loadings (Cu–Zn(A)/ZrO_2, Cu–Zn(B)/ZrO_2, and Cu–Zn(C)/ZrO_2 in Table 1). The results are shown in Fig. 5. The DME conversion followed the trend Cu–Zn(B)/ZrO_2 > Cu–Zn/ZrO_2 > Cu–Zn(C)/ZrO_2 > Cu–Zn(A)/ZrO_2, whereas the selectivity towards the reforming products, H_2 and CO_2 followed the trend Cu–Zn(A)/ZrO_2 > Cu–Zn/ZrO_2 > Cu–Zn(C)/ZrO_2 > Cu–Zn(B)/ZrO_2. These trends cannot be related to a different acidity of the samples (Table 1) and may be due to differences on surface composition and/or contact between Cu, Zn and the support. Additional catalytic tests were carried out over the catalytic monolith Cu–Zn/ZrO_2, where a compromise between activity and selectivity was found. Several DME loads and WHSV values were tested at 753 K with S/C = 1.5 (Table 2). As expected, DME conversion increased as the WHSV decreased from 11.3 to 2.3 L h^{-1} $g_{cat}{}^{-1}$ (from 14.2 to 26.7%) but, interestingly, the increase of DME conversion did not affect the distribution of products, being H_2 and CO_2 the main products of the reaction. In fact, as the contact time increased, the extent of WGS reaction increased, according to a reaction scheme with consecutive reactions, and the amount of CO progressively decreased and that of H_2 and CO_2 increased. Also, a variation of the DME load from 2.7×10^{-3} to 1.1×10^{-2} mol h^{-1} had no significant effect on the product distribution, even at 56% DME conversion.

Table 2
Catalytic performance at 753 K and S/C = 1.5 of the Cu–Zn/ZrO_2 monolith under different DME load and WHSV values.

WHSV (L h^{-1} $g_{cat}{}^{-1}$)	mol_{DME} h^{-1}	Conv. (%)	Selectivity (%)			
			H_2	CO_2	CO	CH_4
2.3	5.3×10^{-3}	26.7	71.8	27.1	0.8	0.3
4.5	5.3×10^{-3}	23.2	71.7	26.2	1.7	0.4
6.8	5.3×10^{-3}	15.0	71.4	26.1	2.1	0.4
9.0	5.3×10^{-3}	13.8	71.5	25.7	2.5	0.4
11.3	5.3×10^{-3}	14.2	71.1	25.7	2.9	0.4
11.3	2.7×10^{-3}	56.0	70.4	25.4	3.7	0.4
11.3	1.1×10^{-2}	10.4	70.9	25.2	3.4	0.4

A stability test was performed over the Cu–Zn/ZrO_2 monolith at 753 K (S/C = 1.5, 2.7×10^{-3} mol_{DME} h^{-1}, WHSV ~16.6 L h^{-1} $g_{cat}{}^{-1}$) and the results were compared with those obtained over Cu/ZrO_2 in order to study the effect of Zn in the stabilization of Cu ensembles over ZrO_2. Fig. 6 shows the yields of H_2, CO_2, CO, and CH_3OH (on a DME converted basis) obtained for each catalytic monolith over time on stream. After a stabilization period of about 3 h, the Cu–Zn/ZrO_2 sample yielded a stable outlet stream with ~5.4 mol H_2/mol DME and ~1.9 mol CO_2/mol DME and a small amount of CO (0.9%) and CH_4 (0.3%). Methanol concentration was less than 50 ppm (the maximum values of mol H_2 and mol CO_2 with respect

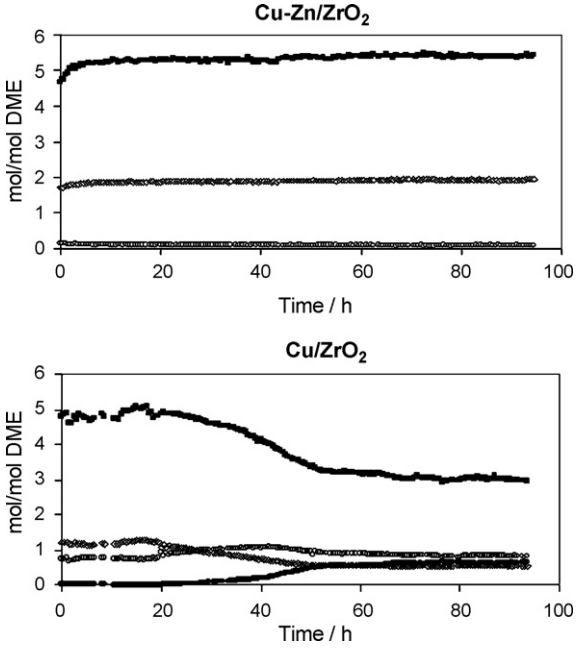

Fig. 6. Stability tests over Cu–Zn/ZrO_2 catalytic monolith (a) and Cu/ZrO_2 catalytic monolith (b) at 753 K (■ = H_2, ◊ = CO_2, ○ = CO, ● = CH_3OH). Experimental conditions: 2.7×10^{-3} mol_{DME} h^{-1}, S/C = 1.5 and WHSV ~16.6 L h^{-1} $g_{cat}{}^{-1}$.

to mol of DME converted as deduced from equation (3) are 6 and 2, respectively). Under these experimental conditions, the catalytic monolith was remarkably stable (Fig. 6a). In contrast, the sample Cu/ZrO_2 deactivated severely over time on stream (Fig. 6b). The decrease in H_2 and CO_2 yields was accompanied by a simultaneous increase in methanol yield. From this behavior, it can be inferred that the deactivation was likely originated by a decrease of Cu active surface area (sintering). This would explain the appearance of methanol due to DME hydration over ZrO_2 and the loss of methanol reforming activity. Therefore, the $Cu–Zn/ZrO_2$ monolith constitutes an active, selective, and stable catalyst for the steam reforming of dimethyl ether. The mild acidity of ZrO_2 is appropriate for DME transformation into methanol without promoting the formation of carbonaceous deposits, Cu is active for methanol reforming, and Zn promotes the WGS reaction and stabilizes the Cu ensembles.

4. Conclusions

Catalytic monoliths containing Cu, Zn, or Cu–Zn supported on CeO_2, ZrO_2, or $CeO_2–ZrO_2$ have been prepared, characterized by SEM, EDX, XRD, NH_3-TPD, and mechanical stability test, and tested in the dimethyl ether (DME) steam reforming reaction under various conditions. DME steam reforming occurred in two steps. First, DME transformed mainly into methanol over acidic sites, and then methanol was efficiently reformed into a mixture of H_2, CO, and CO_2 in the presence of Cu ensembles. ZrO_2-based catalytic monoliths performed better than their CeO_2-based counterparts, both in terms of DME conversion and selectivity into the reforming products, H_2 and CO_2. Monoliths containing $CeO_2–ZrO_2$ support exhibited a poor performance due to low acidity, which was related to the absence of tetragonal ZrO_2. The addition of Zn to supported Cu samples resulted in a strong enhancement of the water gas shift reaction, which lead to a remarkable selectivity improvement in terms of CO transformation into H_2 and CO_2. Among various formulations tested, a $Cu–Zn/ZrO_2$ monolith with [Zr]∼[Cu] + [Zn] wt.% gave the highest H_2 yield. Over this sample, the selectivity was maintained under different DME conversion values obtained by varying the contact time and DME flow rate. A strong positive effect of Zn addition into the catalytic stability of ZrO_2-supported Cu was demonstrated by long-term catalytic tests. Catalyst coatings showed a good mechanical resistance for practical application.

Acknowledgement

This work has been funded through MEC grant ENE2006-06925.

References

[1] V.V. Galvita, G.L. Semin, V.D. Belyaev, T.M. Yurieva, V.A. Sobyanin, Appl. Catal. A 216 (2001) 85–90.
[2] K. Faungnawakij, Y. Tanaka, N. Shimoda, T. Fukunaga, R. Kikuchi, K. Eguchi, Appl. Catal. B 74 (2007) 144–151.
[3] T. Nishiguchi, K. Oka, T. Matsumoto, H. Kanai, K. Utani, S. Imamura, Appl. Catal. A 301 (2006) 66–74.
[4] K. Oka, T. Nishiguchi, H. Kanai, K. Utani, S. Imamura, Appl. Catal. A 309 (2006) 187–191.
[5] K. Takeishi, H. Suzuki, Appl. Catal. A 260 (2004) 111–117.
[6] T.A. Semelsberger, R.L. Borup, J. Power Sources 155 (2006) 340–352.
[7] K. Faungnawakij, T. Fukunaga, R. Kikuchi, K. Eguchi, J. Catal. 256 (2008) 37–44.
[8] K. Faungnawakij, R. Kikuchi, T. Matsui, T. Fukunaga, K. Eguchi, Appl. Catal. A 333 (2007) 114–121.
[9] Y. Tanaka, R. Kikuchi, T. Takeguchi, K. Eguchi, Appl. Catal. B 57 (2005) 211–222.
[10] M. Nilsson, L.J. Pettersson, B. Lindström, Energy Fuels 20 (2006) 2164–2169.
[11] V.A. Sobyanin, S. Cavallaro, S. Freni, Energy Fuels 14 (2000) 1139–1142.
[12] J.J. Zou, C.J. Liu, Y.P. Zhang, Energy Fuels 20 (2006) 1674–1679.
[13] C. Arcoumanis, C. Bae, R. Crookes, E. Kinoshita, Fuel 87 (2008) 1014–1030.
[14] T.A. Semelsberger, R.L. Borup, J. Power Sources 152 (2005) 87–96.
[15] T. Fukunaga, N. Ryumon, S. Shimazu, Appl. Catal. A 348 (2008) 193–200.
[16] T. Mathew, Y. Yamada, A. Ueda, H. Shioyama, T. Kobayashi, Appl. Catal. A 286 (2005) 11–22.
[17] M. Nilsson, P. Jozsa, L.J. Pettersson, Appl. Catal. B 76 (2007) 42–50.
[18] T. Matsumoto, T. Nishiguchi, H. Kanai, K. Utani, Y. Matsumura, S. Imamura, Appl. Catal. A 276 (2004) 267–273.
[19] T.A. Semelsberger, K.C. Ott, R.L. Borup, H.L. Greene, Appl. Catal. A 309 (2006) 210–223.
[20] T.A. Semelsberger, K.C. Ott, R.L. Borup, H.L. Greene, Appl. Catal. B 65 (2006) 291–300.
[21] T.A. Nijhuis, A.E.W. Beers, T. Vergunst, I. Hoek, F. Kapteijn, J.A. Moulijn, Catal. Rev. 43 (4) (2001) 345–380.
[22] A.S. Deshpande, M. Niederberger, Micropor. Mesopor. Mater. 101 (2007) 413–418.
[23] S.T. Korhonen, M.A. Bañares, J.L.G. Fierro, A.O.I. Krause, Catal. Today 126 (2007) 235–247.
[24] H. Wanga, G. Lia, Y. Xueb, L. Lia, J. Solid State Chem. 180 (2007) 2790–2797.
[25] P.H. Matter, U.S. Ozkan, J. Catal. 234 (2005) 463–475.
[26] J. Agrell, H. Birgersson, M. Boutonnoet, I. Melian-Cabrera, R.M. Navarro, J.L.G. Fierro, J. Catal. 219 (2003) 389–403.
[27] J.L.G. Fierro, M. Lo Jacono, M. Inversi, P. Porta, F. Cioci, R. Lavecchia, Appl. Catal. A 137 (1996) 327–348.
[28] Y. Suwa, S. Ito, S. Kameoka, K. Tomishige, K. Kunimori, Appl. Catal. A 267 (2004) 9–16.
[29] N. Iwasa, T. Mayanagi, W. Nomura, M. Arai, N. Takezawa, Appl. Catal. A 248 (2003) 153–160.